# Extension of root-MUSIC to non-ULA Array Configurations

Fabio Belloni, Andreas Richter and Visa Koivunen

Signal Processing Laboratory, SMARAD CoE
Helsinki University of Technology
P.O. Box 3000, FIN-02015 HUT, Finland
Email: {fbelloni,arichter,visa}@wooster.hut.fi

***Abstract*— In this paper we introduce a method for modelling the steering vector of an arbitrary array such that its steering vector can be expressed as the product of a characteristic matrix of the array itself and a vector with a Vandermonde structure containing the unknown parameter. We call this technique manifold separation. By exploiting this concept, we developed a novel version of the root-MUSIC algorithm for Direction of Arrival (DoA) estimation of sources. It can be applied to arbitrary 2-D array configurations. The proposed algorithm processes the data in element-space domain and does not require any transformation or array interpolation. The novel algorithm, named Element-Space root-MUSIC, provides computationally low complexity (search-free) DoA estimation and has close to CRB performance already at low SNRs.**

## I. INTRODUCTION

In array signal processing it is often convenient to work with arrays having a steering vector matrix with a Vandermonde structure. For example, this allows using low complexity Direction of Arrival (DoA) estimators designed for Uniform Linear Arrays (ULA) such as root-MUSIC [1],[5] and root-WSF [2],[3]. Techniques known as array interpolation [1]-[4] and beamspace transform [5]-[7] have been developed in order to map the steering vectors of a planar array onto steering vectors of a ULA-type array, called the virtual array. These preprocessing techniques often introduce mapping errors in the form of bias [2],[6] and excess variance [7]. This leads to DoA estimates which are not statistically efficient.

In this paper we use an alternative approach to this class of problems. Instead of fitting the steering vector of an antenna array onto a previously defined mathematical model [1]-[6], we modify the array model such that the desired Vandermonde structure explicitly appears. The idea is to rewrite the element-space steering vector of a planar array as a product of the characteristic matrix and a Vandermonde structured vector, which depends on the unknown angle of arrival parameter we want to estimate. We will refer to this technique as manifold separation. This approach does not require any division into angular sectors [1] and it provides a significantly smaller fitting error than the other commonly used techniques over the whole $360^\circ$ coverage area. A numerical example demonstrating the benefits of the manifold separation approach over the existing techniques will be presented.

We have applied the manifold separation approach to the DoA estimation problem. We will show that it is possible to perform DoA (azimuth) estimation using a polynomial rooting technique on arbitrary 2-D arrays using the recorded data directly without preprocessing stages. Hence, mapping or interpolation techniques are not longer required. The proposed method works with any antenna array structure, provided that the narrowband model holds and that the antenna array acquires sufficient information on the DoAs of the observed sources. The novel Element-Space root-MUSIC algorithm provides a computationally low complexity (search-free) DoA estimation method and the performance is close to the CRB (Cramèr-Rao Bound) already for low SNRs.

This paper is organized as follows. First, the UCA signal model is presented. In Section III a brief description of the classical mapping techniques, such as the Friedlander interpolation [1] and beamspace transform [5],[6] is given. Then, the concept of manifold separation is introduced. In Section V numerical results of the fitting error resulting from the above techniques are shown. In Section VI, the novel Element-Space root-MUSIC algorithm is described. In Section VII the statistical performance of the proposed algorithm is studied. Finally, Section VIII concludes the paper.

## II. SYSTEM MODEL

Let us have an arbitrary 2-D array of $N$ sensors. There are $P$ ($P < N$) non-coherent narrowband signal sources on the array plane, impinging the array from directions $\phi_1, \phi_2, \ldots, \phi_P$ ($\phi$ is the azimuth angle). Furthermore, we assume that $K$ snapshots are observed by the array. The element-space array output matrix may be written as

$$\mathbf{X} = \mathbf{AS} + \mathbf{N}, \tag{1}$$

where $\mathbf{X} \in \mathbb{C}^{N\times K}$ is the element-space data matrix, $\mathbf{A} \in \mathbb{C}^{N\times P}$ is the element-space steering vector matrix of an arbitrary planar array, $\mathbf{S} \in \mathbb{C}^{P\times K}$ is the source matrix and $\mathbf{N} \in \mathbb{C}^{N\times K}$ contains the measurement noise. The noise is modelled as a stationary, second-order ergodic, zero-mean, spatially and temporally white circular complex Gaussian process.

In this paper we consider the well known Uniform Circular Array (UCA) configuration for azimuth-only estimation. However, this does not limit the generality of the results since any planar array configuration of practical interest may be used as well. The $N \times P$ UCA element-space steering vector matrix may be written as $\mathbf{A} = [\mathbf{a}(\phi_1), \mathbf{a}(\phi_2), \ldots, \mathbf{a}(\phi_P)]$, where each column is of the form

$$\mathbf{a}(\phi_p) = [e^{j\zeta\cos(\phi_p-\gamma_0)}, e^{j\zeta\cos(\phi_p-\gamma_1)}, \ldots, e^{j\zeta\cos(\phi_p-\gamma_{(N-1)})}]^T \tag{2}$$

for $p = 1, 2, \ldots, P$. Here $\zeta = \kappa r \sin\theta$, $r$ is the radius, $\kappa = \frac{\omega}{c}$ is the wavenumber, $c$ is the wave propagation speed, $\omega$ is the angular frequency and $\gamma_n = \frac{2\pi n}{N}$ ($n = 0, \ldots N-1$) is the sensor location. The elevation angle $\theta$ is measured down from the $z$-axis and it is assumed to be fixed, e.g. at $90^\circ$. The azimuth angle $\phi$ is measured counterclockwise from the $x$-axis in the xy-plane.

## III. MAPPING TECHNIQUES

In this section we briefly review the well known array interpolation [1]-[4] and beamspace transform [5]-[7] techniques.

### A. Array interpolation

In array interpolation, the real array manifold (in this case a planar array) is linearly transformed onto a preliminary specified virtual array manifold over a given azimuthal angular sector $\Phi$ [1]-[4]. In

general, the $360^\circ$ coverage area needs to be sectorized into $L$ angular sectors in order to achieve a sufficiently low fitting error [1]-[3]. For the $l^{th}$ angular sector, an interpolation matrix $\mathbf{B}_l$ is designed as

$$\mathbf{B}_l \mathbf{a}(\phi) \approx \widetilde{\mathbf{a}}(\phi) \qquad \text{for} \quad \phi \in \Phi \ , \tag{3}$$

where $\mathbf{a}(\phi)$ and $\widetilde{\mathbf{a}}(\phi)$ are the $N \times 1$ and $\widetilde{N} \times 1$ steering vectors of the real and the virtual array, respectively. Notice that usually $\widetilde{\mathbf{a}}(\phi)$ corresponds to a ULA steering vector.

The interpolation matrix $\mathbf{B}_l$ is found as the Least Squares (LS) solution. This has to be done only once for each sector and can be performed offline. In [2]-[4], discussions about reducing the condition number of the interpolation matrix $\mathbf{B}_l$ are carried out. Moreover, in case of array interpolation also the design of the virtual array is an issue because the virtual array (ULA) can be interpreted as a physical array [4]. Hence, the location of the virtual array with respect to the real array, its orientation, the number of elements $\widetilde{N}$, and the interelement spacing have to be properly chosen to provide as small as possible fitting error.

An example for bias reduction in DoA estimation algorithms using array interpolation can be found in [2], where an optimal mapping from circular to linear manifold is proposed.

### *B. Beamspace Transform*

The Beamspace Transform (BT) [5],[6] is a modal transform that maps the $N \times 1$ steering vector of a UCA $\mathbf{a}(\phi)$ into $\mathcal{M} \times 1$ Vandermonde structured steering vectors of a ULA-type array $\mathbf{a}_v(\phi)$. The mapping is performed similarly to [3],[5]-[7] by

$$\mathbf{F}_e^H \mathbf{a}(\phi) \approx \mathbf{a}_v(\phi) \ . \tag{4}$$

The BT does not require division into sectors, and it works over the whole $360^\circ$ coverage area. The $\mathcal{M} \times N$ beamformer $\mathbf{F}_e^H$, which maps the observed signal approximately from the UCA-manifold to the ULA-manifold is a DFT matrix [3],[5],[6]. The modes that can be excited are $m \in \{-M, \ldots, 0, \ldots, M\}$ and $\mathcal{M} = 2M+1$ defines the size of the virtual array.

The transform in (4) is approximative and the transformation error can be neglected only when certain conditions (number of elements, interelement spacing, SNR, etc.) are fulfilled [5],[6]. This leads to both a fitting error between the planar array and the virtual array, see Fig. 2, and a deterioration in the statistical performance of the DoA algorithm [6]. A solution to this problem can be found in [6],[7].

In contrast to the array interpolation technique, Section III-A, the beamspace transform does not perform mapping between a real planar array and a "physical" linear array. Instead, it exploits some mathematical relationships in order to rewrite the product between the beamformer and the manifold of the real array into other terms which explicitly show the desired Vandermonde structure [3],[5]-[7].

## IV. Manifold Separation

To our best knowledge, the idea of manifold separation for arbitrary 2-D array configurations of omnidirectional sensors was first introduced in [8] in the context of wideband processing [3],[8]. In this paper we reformulate the problem and present a practical way (through IDFT) of performing manifold separation, which could also be used on arbitrary 2-D array configurations of both directional and omnidirectional sensors [9]. The goal is to derive a search-free DoA estimation algorithm for arbitrary planar arrays, which works on the element-space domain.

The key idea of the manifold separation method is to rewrite the element-space steering vector of a planar array as a product of a matrix characteristic for the array itself and a Vandermonde structured vector, which depends on the azimuth angle. No interpolation (or mapping) of the planar array steering vector is needed, anymore. Instead, we change the data model of the planar array such that a term with a Vandermonde structure is formed. Similarly to the beamspace transform, the manifold separation method does not need to divide the whole $360^\circ$ coverage into angular sectors.

In addition to [8], we show two alternative ways to perform the manifold separation. The first approach solves a LS problem, while the second uses the Effective Aperture Distribution Function (EADF) [7],[9] of the planar array. These approaches lead to the same result.

The manifold separation may be rewritten as a LS problem as:

$$\arg\min_{\mathbf{G}} \Big\{ \sum_{t=1}^{T} \Big\| \mathbf{a}(\phi_t) - \mathbf{G}\mathbf{d}(\phi_t) \Big\|_F^2 \Big\} \ , \tag{5}$$

where $\mathbf{G}$ is the $N \times \widetilde{\mathcal{M}}$ characteristic matrix, $\widetilde{\mathcal{M}}$ is the number of selected modes, $\mathbf{a}(\phi_t)$ is the $N \times 1$ element-space steering vector of the planar array and $\mathbf{d}(\phi)$ is the $\widetilde{\mathcal{M}} \times 1$ Vandermonde vector

$$\mathbf{d}(\phi) = \big[ e^{-j\frac{\widetilde{\mathcal{M}}-1}{2}\phi}, \ldots, e^{-j\phi}, 1, e^{j\phi}, \ldots, e^{j\frac{\widetilde{\mathcal{M}}-1}{2}\phi} \big]^T \ . \tag{6}$$

The characteristic matrix $\mathbf{G}$ provides a mathematical model of the narrowband array. It contains a sufficiently accurate description of elements characteristic, positions and manufacturing errors of the antenna array.

The optimization problem in eq. (5) can be solved by choosing $T \gg N$ directions $\phi_t$ uniformly distributed over $[0, 2\pi)$. We collect the steering vectors of the planar array for the set of angles $\phi_1, \ldots, \phi_T$ in a $N \times T$ matrix $\mathbf{A} = [\mathbf{a}(\phi_1), \ldots, \mathbf{a}(\phi_T)]$. Similarly, we can form the $\widetilde{\mathcal{M}} \times T$ matrix $\widetilde{\mathbf{D}} = [\mathbf{d}(\phi_1), \ldots, \mathbf{d}(\phi_T)]$. The matrix $\mathbf{G}_{LS}$ minimizing the sum of squared errors can be found as

$$\mathbf{G}_{LS} = \mathbf{A}\widetilde{\mathbf{D}}^H (\widetilde{\mathbf{D}}\widetilde{\mathbf{D}}^H)^{-1} \ . \tag{7}$$

Note that by taking $T \geq \widetilde{\mathcal{M}}$ distinct directions $\phi_t$, the inverse in eq. (7) always exist. Unlike in array interpolation techniques, the matrix $\widetilde{\mathbf{D}}$ has full row rank and no approximation errors occur during the matrix inversion.

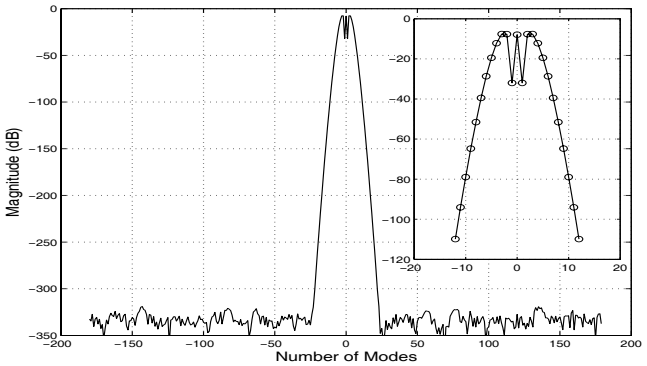


Fig. 1. Magnitude of the $n^{th}$ array element characteristic for a UCA with $N = 8$ sensors, radius $r = 0.6\lambda$ and $T = 360$ points ($n^{th}$ row of $\mathbf{G}$ in (5)).

The characteristic matrix $\mathbf{G}$ can also be computed by using the concept of EADF [9]. It represents the inverse Fourier transform of the array response to a far field source, which moves around the array at a fixed elevation angle (e.g. $\theta = 90^\circ$) along the azimuthal direction over the range $\phi \in [0, 2\pi)$ [7]. A discrete set of measured points along the direction $\phi$ is then recorded. This leads to a discrete periodic function with period $2\pi$ in azimuth. Hence, the EADF can be expressed by the IDFT (Inverse Discrete Fourier Transform) of the measured data set. It represents a sufficiently accurate description of the real-world array including array imperfections. For the $q^{th}$ row

of the matrix $\mathbf{A}$, the element $\widetilde{g}_{q\mu}$ of the $N \times \widetilde{\mathcal{M}}$ EADF matrix $\widetilde{\mathbf{G}}$ is the $T$-points IDFT

$$\widetilde{g}_{q\mu} = \frac{1}{T} \sum_{t=1}^{T} a_{qt} \; e^{j\frac{2\pi}{T}(t-1)(\mu-1)} \; , \tag{8}$$

for $1 \leq \mu \leq \widetilde{\mathcal{M}}$ and $j = 1, \ldots, N$. The computation of the matrix $\mathbf{G}$ in eq. (5) can be carried out either by solving the LS problem (7) or by computing the EADF matrix in (8). Observe that $\mathbf{G}_{LS} = \widetilde{\mathbf{G}}$ holds if the angles $\phi_1, \ldots, \phi_T$ are chosen such that $\widetilde{\mathbf{D}}$ in eq. (7) is a DFT matrix. In Fig. 1 we show the $n^{th}$ row of $\mathbf{G}$, which represents the $n^{th}$ array element characteristic for a UCA [7].

There are important differences among the concepts of array interpolation, beamspace transform, and manifold separation presented so far. The first two techniques always require mapping from a real array to a virtual array with equal or smaller number of elements, i.e. $N \geq \widetilde{N}$ or $N \geq \mathcal{M}$ [3],[5]. However, this does not apply to the manifold separation technique. In fact, we are not mapping or interpolating from one steering vector structure (e.g. UCA) to another (e.g. ULA). We rather change the array model by using a more flexible mathematical formulation. Hence, we are free to decide the dimension of the $\widetilde{\mathcal{M}} \times 1$ Vandermonde structured vector $\widetilde{\mathbf{d}}(\phi)$ such that $N \ll \widetilde{\mathcal{M}}$. Theoretically, we can choose up to $\widetilde{\mathcal{M}} = T$, but in practice it is sufficient to choose $N < \widetilde{\mathcal{M}} \ll T$ as shown in Table I. Here we give a numerical example showing the fitting error in eq. (11) as a function of $\widetilde{\mathcal{M}}$ when a UCA with $N = 8$ sensors and $T = 360$ calibration points is used. Clearly, the error decreases rapidly as $\widetilde{\mathcal{M}}$ increases. Then, when the fitting error reaches the computational accuracy of the used machine (IEEE-754, 64 bit float), it saturates.

TABLE I

ERROR FITTING IN CASE OF MANIFOLD SEPARATION AS A FUNCTION OF $\widetilde{\mathcal{M}}$. THE ERROR DECREASES RAPIDLY AS $\widetilde{\mathcal{M}}$ INCREASES.

| $N$ | $\widetilde{\mathcal{M}} = 7$ | $\widetilde{\mathcal{M}} = 9$ | $\widetilde{\mathcal{M}} = 25$ | $\widetilde{\mathcal{M}} = 45$ | $\widetilde{\mathcal{M}} = 359$ |
|---|---|---|---|---|---|
| 8 | 0.1262 | 0.0241 | $0.7677e-8$ | $1.2185e-16$ | $5.8796e-17$ |

## V. COMPARISON OF FITTING ERRORS

In this section we show some numerical results, which clearly show that the fitting error given by the manifold separation technique is significantly smaller than the one given either by array interpolation [1]-[3] or beamspace transform [5],[6]. In the example depicted in Fig. 2, we have used an UCA with $N = 8$ sensors and radius $r = \frac{\lambda}{2}$.

In case of array interpolation, a $30^\circ$ wide angular sector having $\phi \in [75^\circ, 105^\circ]$ and $Q = 2049$ calibration points have been considered. The UCA is mapped onto a virtual array with size $\widetilde{N} = 7$ and located along its diameter. At both ends, the two virtual array elements are placed on the circumference of the UCA. Hence, the interelement spacing is $d = \frac{2r}{\widetilde{N}-1}$. The orientation of the virtual ULA is chosen such that its broadside direction is in the middle of the angular sector. Note that with this configuration, and for sources located within the considered sector, the UCA and virtual ULA have approximatively the same aperture. The interpolation matrix $\mathbf{B}_l$ used in the simulation has a condition number of $\approx 19$dB. Fig. 2 shows that the array interpolation technique provides a low fitting error within the selected sector, but a large error elsewhere.

In case of beamspace transform, we have considered a virtual array of size $\mathcal{M} = 7$. In this case, the mapping is performed over the whole $360^\circ$ coverage area. In Fig. 2 we can see the fitting error provided by this technique. It shows uniform performance along the visible area.

Finally, we have studied the performance of the manifold separation method. In the simulation we have formed a grid of $T = 360$ calibration points uniformly distributed along the whole $360^\circ$ coverage area. We have considered a Vandermonde structured vector $\mathbf{d}(\phi)$ of size $\widetilde{\mathcal{M}} = 37$. In Fig. 2 we can see that the manifold separation approach provides a fitting error which is several orders of magnitude smaller than the error given by the other two techniques.

The normalized fitting errors used in Fig. 2 are

$$e_{ai}(\phi) = \left\| \mathbf{B}\mathbf{a}(\phi) - \widetilde{\mathbf{a}}(\phi) \right\|_F \Big/ \left\| \widetilde{\mathbf{a}}(\phi) \right\|_F \tag{9}$$

$$e_{bt}(\phi) = \left\| \frac{1}{\sqrt{N}} \mathbf{J}_\zeta^{-1} \mathbf{F}_e^H \mathbf{a}(\phi) - \mathbf{d}(\phi) \right\|_F \Big/ \left\| \mathbf{d}(\phi) \right\|_F \tag{10}$$

$$e_{ms}(\phi) = \left\| \mathbf{G}\mathbf{d}(\phi) - \mathbf{a}(\phi) \right\|_F \Big/ \left\| \mathbf{a}(\phi) \right\|_F \; , \tag{11}$$

where $\phi \in [0, 2\pi)$ and $e_{ai}(\phi)$, $e_{bt}(\phi)$ and $e_{ms}(\phi)$ stands for the errors fitting obtained by array interpolation, beamspace transform and manifold separation, respectively.

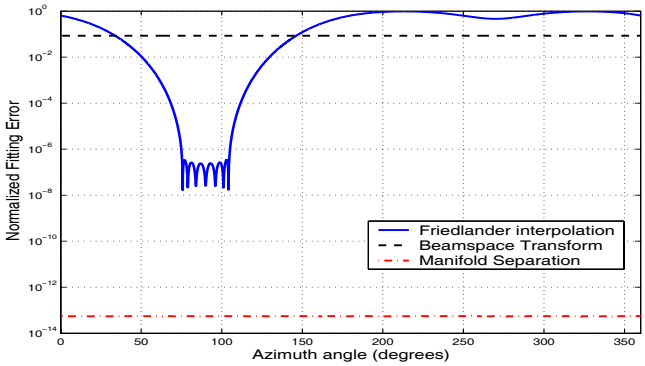


Fig. 2. Fitting error comparison. The manifold separation method provides a significant and consistently smaller error than the conventional techniques over the whole coverage area.

## VI. ELEMENT-SPACE ROOT-MUSIC

In this section we apply the manifold separation approach to derive a novel version of the root-MUSIC algorithm for DoA estimation of non-coherent sources. It can be used on arbitrary array configurations. The proposed method allows azimuthal DoA estimation at a fixed elevation angle. We will refer to this novel algorithm as Element-Space root-MUSIC.

In contrast to the well known interpolating and beamspace rooting techniques [1]-[6], the data recorded by the planar array are neither interpolated nor mapped onto another array configurations or domain. Instead, by using the manifold separation technique (see Section IV), we can directly apply the root-MUSIC algorithm on the recorded data. In contrast to interpolation or mapping techniques, the systematic error [2],[6] and the excess variance [6] can be made arbitrarily small by choosing a sufficiently large number of modes $\widetilde{\mathcal{M}}$ (see Table I).

By exploiting the concept of manifold separation, we can rewrite the element-space steering vector of an arbitrary planar array as

$$\mathbf{a}(\phi) = \mathbf{G}\mathbf{d}(\phi) + \mathcal{O}(\widetilde{\mathcal{M}}) \; , \tag{12}$$

where $\mathcal{O}(\widetilde{\mathcal{M}})$ represents a modelling error, which may be made as small as desired only by increasing $\widetilde{\mathcal{M}}$. Note that in a real-world scenario whenever the SNR $\ll \min_{\phi}(\|\mathbf{a}(\phi)\|)/\mathcal{O}(\widetilde{\mathcal{M}})$, the residual modelling error can be neglected and eq. (12) still holds. In eq. (12), $\mathbf{G}$ is the $N \times \widetilde{\mathcal{M}}$ characteristic matrix, which may be computed either as the solution of the LS problem in eq. (7) or as EADF of the planar array, see eq. (8).

Consequently, we can rewrite the system model in eq. (1) as

$$\mathbf{X} = \mathbf{AS} + \mathbf{N} = \mathbf{GDS} + \mathbf{N} \ , \tag{13}$$

where $\mathbf{D}$ is a $\widetilde{\mathcal{M}} \times P$ matrix formed as $\mathbf{D} = [\mathbf{d}(\phi_1), \ldots, \mathbf{d}(\phi_P)]$ and $\phi_1, \ldots, \phi_P$ are the true DoAs of the $P$ non-coherent sources.

The element-space array covariance matrix can be expressed by

$$\mathbf{R}_x = \mathbf{AR}_S\mathbf{A}^H + \sigma_\eta^2\mathbf{I} = \mathbf{GDR}_S\mathbf{D}^H\mathbf{G}^H + \sigma_\eta^2\mathbf{I} \ , \tag{14}$$

where $\mathbf{I}$ and $\mathbf{R}_S$ are the $N \times N$ identity and the $P \times P$ signal covariance matrices, respectively. Furthermore, by expressing eq. (14) in terms of eigenvalue decomposition we get

$$\mathbf{R}_x = \mathbf{E}_S\Lambda_S\mathbf{E}_S^H + \sigma_\eta^2\mathbf{E}_\eta\mathbf{E}_\eta^H \ . \tag{15}$$

Here $\mathbf{E}_S$ and $\mathbf{E}_\eta$ span the $N \times P$ signal and the $N \times (N-P)$ noise subspaces, respectively. Note that $\mathbf{E}_S$, $\mathbf{A}$ and $\mathbf{GD}$ span the same subspace. Consequently, $\mathbf{GD}$ is orthogonal to the noise subspace $\mathbf{E}_\eta$. This relationship is used in the derivation of the proposed Element-Space root-MUSIC algorithm.

By assuming that all the $P$ sources are at the same elevation angle, the Element-Space MUSIC pseudo-spectrum can be expressed as

$$S_{music}(\phi) = \left(\mathbf{a}^H(\phi)\mathbf{E}_\eta\mathbf{E}_\eta^H\mathbf{a}(\phi)\right)^{-1}, \tag{16}$$

where $\mathbf{a}(\phi)$ is the $N \times 1$ UCA element-space steering vector. The DoAs may then be computed by performing an exhaustive search for the local peaks in the range $\phi \in [0, 2\pi)$, which has clearly high computational complexity [5],[8]. However, by exploiting the concept of manifold separation, we can reduce the complexity. We can rewrite eq. (16) in a form which allows fast (search-free) polynomial rooting algorithms to be applied, namely

$$S_{music}(\phi) = \left(\mathbf{d}^H(\phi)\mathbf{G}^H\mathbf{E}_\eta\mathbf{E}_\eta^H\mathbf{Gd}(\phi)\right)^{-1} \ . \tag{17}$$

In fact, from eq. (17) we can clearly observe that we have restored the desired Vandermonde structure without performing any mapping or interpolation of the recorded data. Note that in order to preserve the uniqueness of the roots associated with the true DoAs and avoiding spurious roots on the unit circle, the following condition has to be fulfilled:

$$\mathbf{Gd}(\phi_i) \neq \mathbf{Gd}(\phi_j) \ , \tag{18}$$

for $\phi_i \neq \phi_j$ and $\phi \in [0, 2\pi)$. Hence, with $\mathbf{E}_g = \mathbf{G}^H\mathbf{E}_\eta\mathbf{E}_\eta^H\mathbf{G}$, the pseudo-spectrum in eq. (17) can be rewritten as

$$F_{root-MUSIC}(\phi) = \sum_{l=-(\widetilde{\mathcal{M}}-1)}^{\widetilde{\mathcal{M}}-1} c(l)e^{jl\phi} \tag{19}$$

where $c(l) = \sum_{i,j:j-i=l} \mathbf{E}_g(i,j)$. Therefore, by substituting $z = e^{j\phi}$ into the $\widetilde{\mathcal{M}} \times 1$ Vandermonde structured vector $\mathbf{d}(\phi)$, the pseudo-spectrum in eq. (17) can be rewritten in polynomial form as

$$c(\widetilde{\mathcal{M}}-1)z^{2\widetilde{\mathcal{M}}-2} + c(\widetilde{\mathcal{M}}-2)z^{2\widetilde{\mathcal{M}}-3} + \ldots + c(-\widetilde{\mathcal{M}}+1) = 0 \ , \tag{20}$$

where the phase angles of the $P$ roots closest to the unit circle $z_p$ will yield the azimuth estimates $\phi_p = \angle(z_p)$ of sources at a given elevation angle.

## VII. Simulation Results

In this section we present simulation examples in order to demonstrate the performance of the proposed Element-Space root-MUSIC algorithm. We have simulated a UCA with $N = 8$ sensors, radius $r = 0.6\lambda$, interelement spacing $d \simeq 0.4592\lambda$, $K = 256$ recorded snapshots and two uncorrelated sources located at $(\phi_1, \phi_2) = (25^\circ, 35^\circ)$.

In Fig. 3, the statistical performance of the algorithm using 2000 independent Monte Carlo trials for each SNR, is shown. The algorithm is close to the CRB already for low SNRs. Unlike the array interpolation and beamspace transform techniques, the statistical performance of the algorithm is also close to the CRB for high SNRs. This shows that no significant systematic error [2],[6],[7] is introduced by the manifold separation technique.

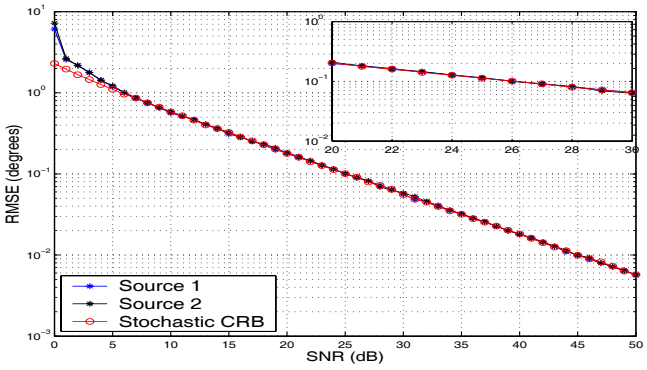


Fig. 3. Statistical performance of the proposed Element-Space root-MUSIC algorithm. At low SNRs the algorithm is already close to the CRB. At high SNRs, no systematic error (error floor) is introduced by manifold separation.

## VIII. Conclusions

In this paper a novel version of root-MUSIC algorithm for DoA estimation of non-coherent sources has been introduced. It can be used on arbitrary 2-D array configurations, which are appropriate for the problem at hand. The novel algorithm provides asymptotically optimal, computationally low complexity (search-free) DoA estimation and has very good statistical performance. The algorithm uses the manifold separation technique. We have compared the manifold separation technique with well know methods used in DoA estimation such as array interpolation and beamspace transform.

## References


[1] Friedlander, B.; *The root-MUSIC algorithm for direction finding with interpolated arrays*. Signal Processing, Vol. 30, 1993, Page(s): 15-29.

[2] Hyberg, P.; Jansson, M.; Ottersten, B.; *Array interpolation and bias reduction*. IEEE Tr. Signal Processing, Vol. 52 Issue: 10, October 2004, Page(s): 2711-2720.

[3] Lau, B.K.; *Applications of Antenna Arrays in Third-Generation Mobile Communications*. Ph.D. Thesis, Curtin University of Technology, Perth, Australia, 2002.

[4] Buhren, M.; Pesavento, M.; Böhme, J.F.; *Virtual array design for array interpolation using differential geometry*. Proc. of IEEE International Conference on Acoustics, Speech, and Signal Processing, ICASSP'04, Vol. 2, 17-21 May 2004, Page(s): ii-229-32.

[5] Mathews, C.P., Zoltowski, M.D., *Eigenstructure techniques for 2-D angle estimation with uniform circular arrays*. IEEE Tr. Signal Processing, Vol. 42 No. 9, 1994, Page(s): 2395-2407.

[6] Belloni, F.; Koivunen, V.; *Beamspace Transform for UCA: Error Analysis and Bias Reduction*. Technical Report No.48, ISBN: 951-22-7292-X, Signal Processing Laboratory, Helsinki University of Technology, 2004. (Accepted in Sept. 2005, to appear in the IEEE Tr. Signal Processing.)

[7] Belloni, F.; Richter, A.; Koivunen, V.; *Reducing Excess Variance in Beamspace Methods for Uniform Circular Array*. Proc. of the IEEE Workshop on Statistical Signal Processing, France, July 17-20, 2005.

[8] Doran, M.A.; Doron, E.; Weiss, A.J.; *Coherent Wide-Band Processing for Arbitrary Array Geometry*. IEEE Tr. Signal Processing, Vol. 41, Issue 1, January 1993, Page(s):414-417.

[9] Thoma, R.S.; Landmann, M.; Sommerkorn, G.; Richter, A.; *Multidimensional high-resolution channel sounding in mobile radio*. Proc. of the $21^{st}$ IEEE Instrumentation and Measurement Technology Conference, IMTC'04, Vol. 1, 18-20 May 2004, Page(s): 257-262.